Supplementary Information for

Resistive Switching of Alkanethiolated Nanoparticle Monolayers Patterned by Electron-Beam Exposure

Patrick A. Reissner[a], Yuriy Fedoryshyn[b], Jean-Nicolas Tisserant[a], Andreas Stemmer[a]**

a ETH Zürich, Nanotechnology Group, Säumerstrasse 4, CH-8803 Rüschlikon, Switzerland

b ETH Zürich, Institute of Electromagnetic Fields, Gloriastrasse 35, CH-8092 Zürich, Switzerland

Contents

I. Raman spectroscopy

II. Examples of failed development procedures

III. Fabrication of electrodes

IV. Statistics of set voltage

V. Coulomb blockade in nanoparticle structures

VI. Current measurement over time at constant voltage

VII. Resistive switching for larger compliance current

VIII. Electric breakdown in 30-nm junctions

IX. Instrumentation

X. Reversible Switching

I. Raman Spectroscopy

Fig. S1 shows a normalized Raman spectrum of a pristine and an exposed monolayer of alkanethiol-stabilized 10-nm gold nanoparticles. The ν_s(C-C) bands at 1064 cm^{-1}, 1083 cm^{-1} and 1128 cm^{-1} are clearly present in the spectra of the pristine sample and disappear after exposure.[1] The decline of the $\nu_t((CH_2)_n)$ band at 1296 cm^{-1} provides further evidence for the depletion of alkane chains upon exposure.[2] However, no difference in the intensity of the C-H region between 2853 cm^{-1} and 2963 cm^{-1} in Fig. S2 can be observed.[1] Therefore, a transformation of alkane chains into an amorphous carbon phase is expected. The spectra shown in Fig. S1 were measured with a Renishaw inVia Raman microscope, using a laser wavelength of 785 nm at a power of 0.3 mW and a 50× magnification objective. The measurement time was set to 60 s. The spectra are normalized with a spectrum measured of the SiO2/Si substrate. The data shown in Fig. S2 was measured with a WiTEC Raman microscope at a laser wavelength of 532 nm. A laser power of 5 mW and a 10× magnification objective were chosen. The measurement time was 10 s. In both figures, the black spectrum is shifted in y- direction for clarity.

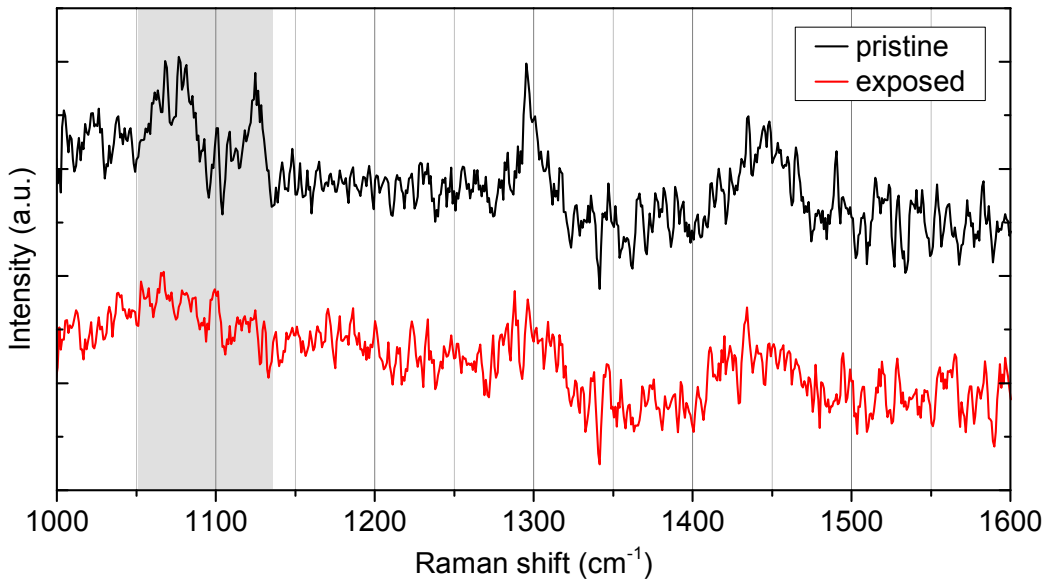

Fig. S1 Raman spectra of a pristine (black) and electron-beam exposed (red) gold nanoparticle monolayer. The gray shaded area highlights the region of ν_s(C-C) bands.

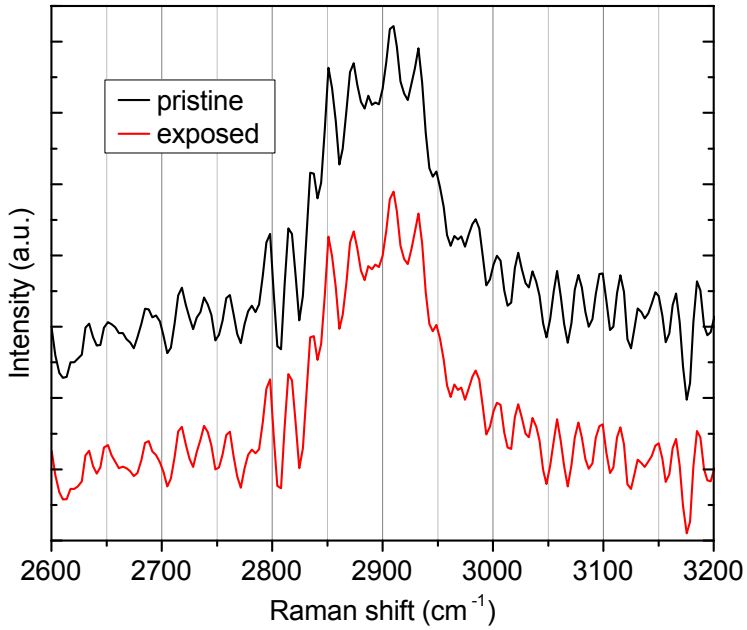

Fig. S2 Raman spectra of a pristine (black) and electron-beam exposed (red) gold nanoparticle monolayer.

II. Examples of failed development procedures

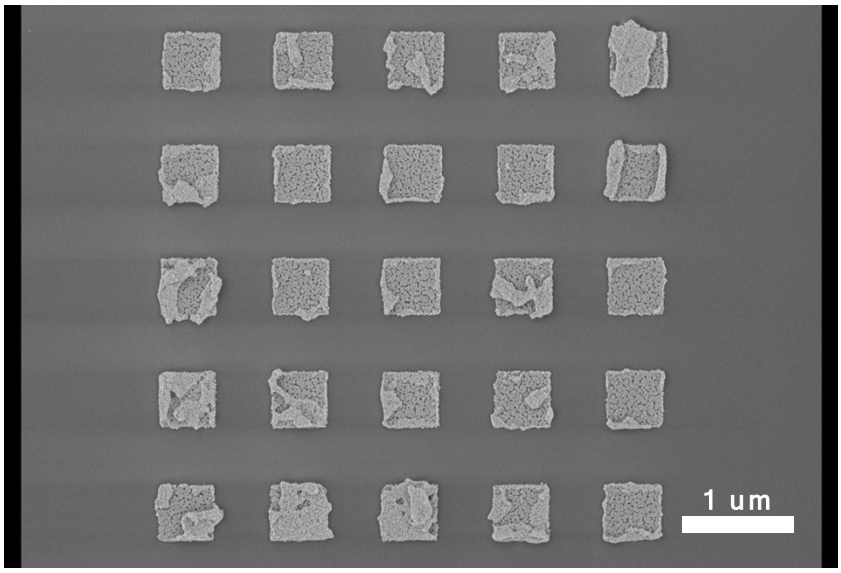

Fig. S3 SEM image of square patterns of a gold nanoparticle monolayer made by electron-beam exposure and subsequent development. The sample was directly immersed into a mixture of ammonia and THF instead of water first. The formation of double- and multilayers on top of the squares is clearly visible.

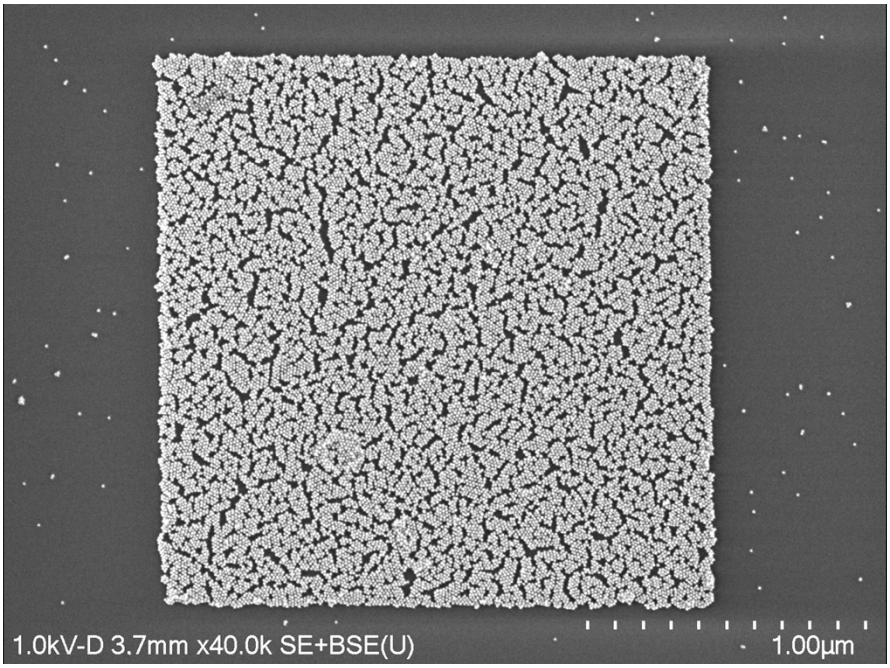

Fig. S4 SEM image of a square pattern of a gold nanoparticle monolayer made by electron-beam exposure and subsequent development. The sample was first immersed in water. Pure THF was added to lift-off unexposed nanoparticles. It is clearly visible that many nanoparticles remain in the unexposed area.

III. Fabrication of electrodes

Gold electrodes were fabricated in two steps. First, we made macroscopic contacts with a height of 80 nm. Subsequently these electrodes were extended by 20 nm high contacts to avoid the formation of cracks in the nanoparticle monolayer during deposition. In both cases, electrode patterns were written with a Vistec EBPG5200 e-beam in a MMA/PMMA layer. Subsequent development in 1:2 solution of methyl-isobutyl-ketone and isopropyl alcohol was followed by electron-beam evaporation of gold. We used N-Methyl-2-pyrrolidone for the lift-off process.

IV. Statistics of set voltage

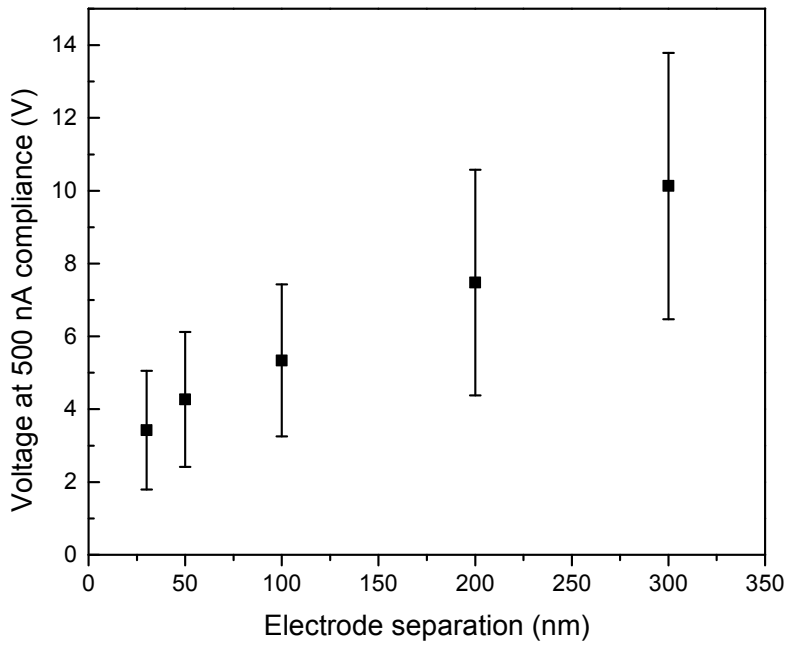

Fig. S5 The voltage to reach a 500 nA compliance current was measured for 80 devices with different electrode separations of 30 nm, 50 nm, 100 nm, 200 nm and 300 nm. The mean voltage and standard deviation are shown for corresponding electrode separations.

The configuration of nanoparticles between electrodes varies similarly to the lines shown in Figure 2a in the main manuscript, leading to a variation in initial device resistance. Similar variations in resistance are also observed for alkanethiol stabilized nanoparticle monolayers. We could not find a correlation between the number of particles and the set current. We believe that small variations in the interparticle distance originating from the self-assembly process significantly influence device resistance.

V. Coulomb blockade in nanoparticle structures

Nonlinear I-V behavior due to Coulomb blockade in nanoparticle networks only occurs if the relation $E_c > k_bT$ is valid. E_c is the charging energy for nanoparticle arrays and can be approximated by the following equation.[3]

$$E_c = \frac{e^2}{8\pi\varepsilon_0\varepsilon_r R(R+s)} \quad s$$

Even though the relative permittivity ε_r for amorphous carbon is 5.5 (or lager), an upper boundary of E_c is calculated for $\varepsilon_r = 3$. For our nanoparticle radius R = 5 nm and separation s = 3 nm, we find $E_c < 18$ meV, which is well below k_bT at room temperature. Therefore, a linear I-V behavior can be expected at low voltages for our structures. We applied a continuous voltage sweep to measure the current response in the pA regime (Fig. S6) for a 30-nm and a 500-nm wide device. Both I-V curves show no sign of Coulomb blockade.

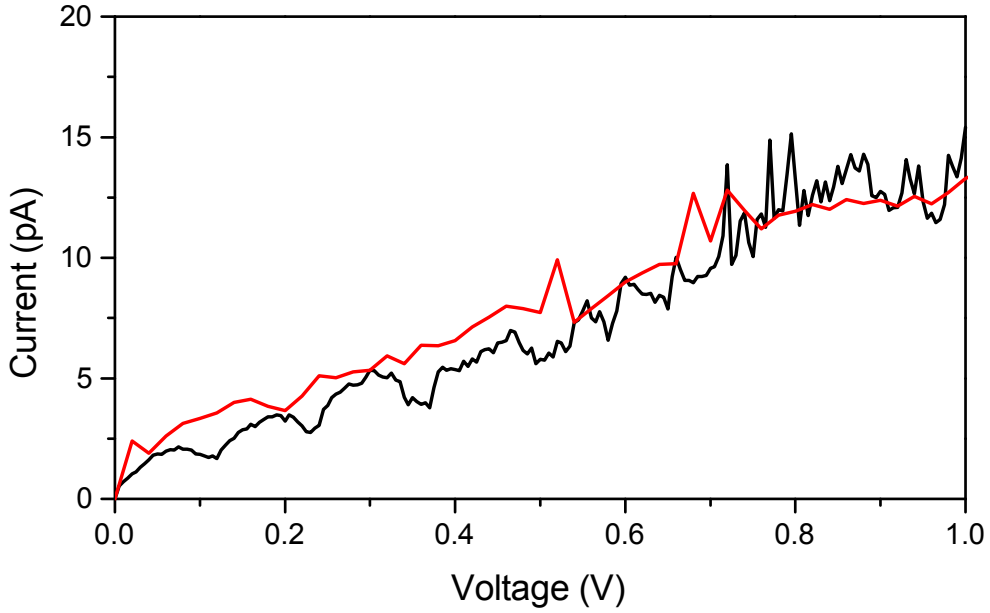

Fig. S6 Continuous voltage sweep for a 30-nm (red) and 500-nm (black) wide device in the initial state.

VI. Current measurement over time at constant voltage

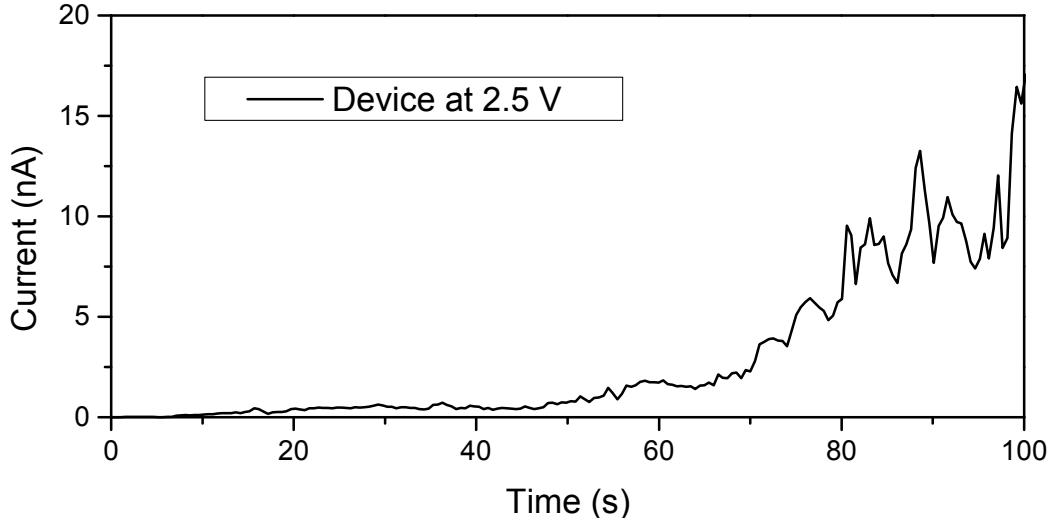

Fig. S7 Gradually increasing current over time for a device at a constant voltage of 2.5 V.

VII. Resistive switching for a large compliance current

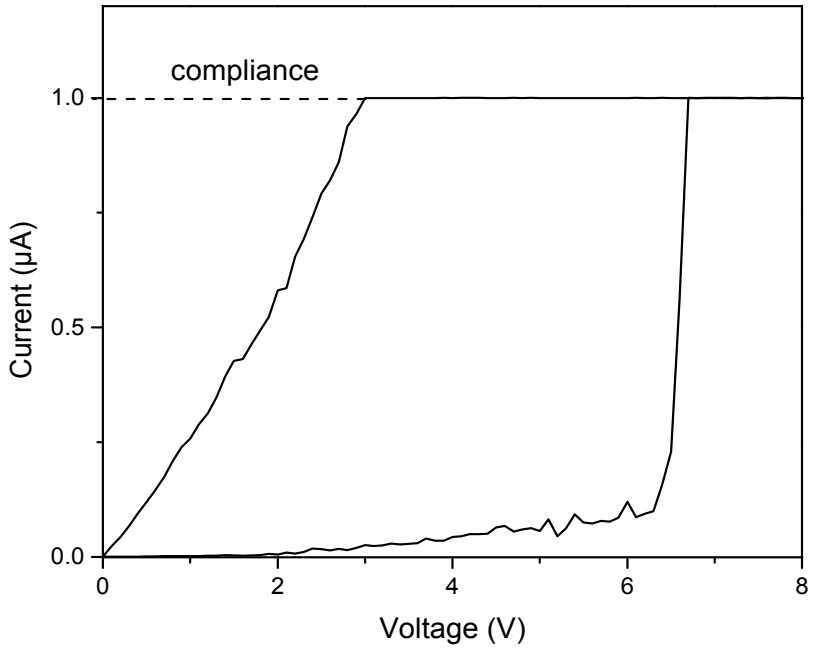

Fig. S8 Bidirectional pulsed voltage sweep between 0 V to 8 V with 1 μA compliance.

VIII. Electric breakdown in 30-nm junctions

We tested devices with an electrode separation of 30 nm without nanoparticles. No sign of resistive switching was observed in the pulsed voltage sweep up to 20 V shown in Fig. S9. This excludes a dielectric breakdown to be the reason for the observed switching in nanoparticle-based devices.

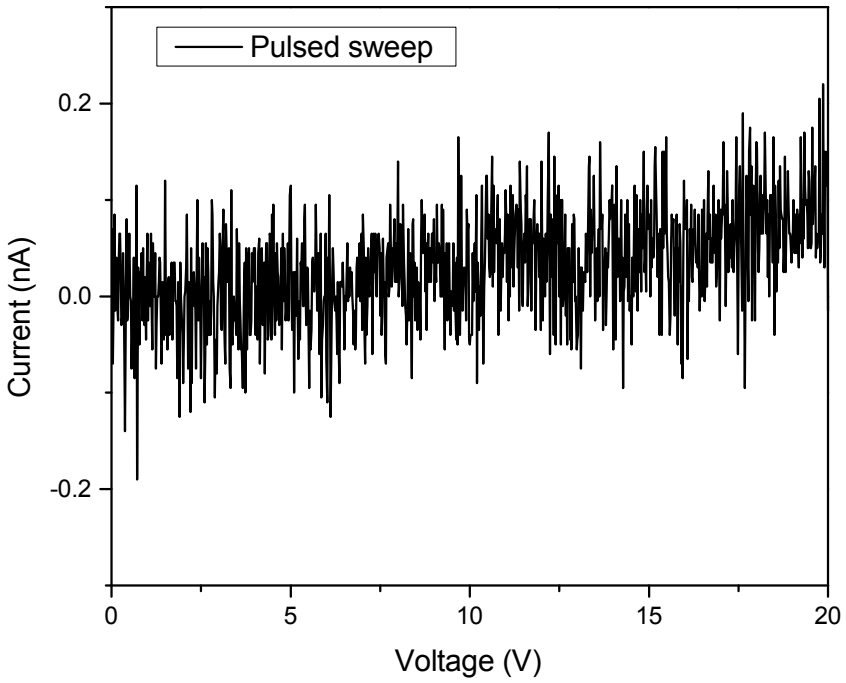

Fig. S9 Pulsed voltage sweep from 0 V to 20 V applied to a device with 30 nm electrode separation in the absence of gold nanoparticles between the electrodes.

In addition to our measurements, we address the question of electric breakdown in our devices more fundamentally by summarizing results from literature:

i) Breakdown of air between metallic electrodes

The Paschen law describes the dielectric breakdown voltage of air depending on the electrode separation. However, for gaps smaller than a few μm strong deviations were found from the Paschen law.[4] In the range of nanometer-sized gaps, Fowler-Nordheim field emission is the dominating mechanism.

Extrapolation of the data for gold electrodes by Peschot *et al.*[4] results in a breakdown voltage above 20 V for 30 nm separation. Further studies show that the breakdown voltage strongly increases when the voltage is applied in pulses rather than as a DC bias.[5] As stated in the manuscript we only applied pulses of 20 ms for sweeps to higher voltages. DC sweeps were only applied at lower voltages up to 2 V.

Furthermore, a breakdown would create substantial damage to the electrodes, which we did not observe in SEM images.

ii) Breakdown of SiO_2 between metallic electrodes

It is known from literature that thermally grown SiO_2 breaks down at field strengths above 8 MV/cm.[6] Our devices were fabricated on top of 1 µm thick thermally grown SiO_2. Even though we observed resistive switching much below 20 V we shall take this value to estimate the electric field strength. Applying 20 V to one electrode the electric field strength between the electrode and the silicon substrate is about 51 kV/cm. The field strength between electrodes with a separation of 30 nm is about 1.7 MV/cm at 20 V, which is much below the breakdown field for thermally grown SiO_2, considering the exponential dependence of the breakdown probability on the electric field strength. Larger local field strengths at electrode edges are not expected to exceed 6 MV/cm.

Additionally, the breakdown probability decreases exponentially with the time of the applied bias.[6] We exclusively applied 20 ms pulses to observe resistive switching in our devices.

IX. Instrumentation

Scanning electron microscopy images were taken with a Hitachi SU8200 SEM. Devices were tested on a Signatone probe station with a Keysight B2912A precision source / measure unit.

X. Reversible Switching

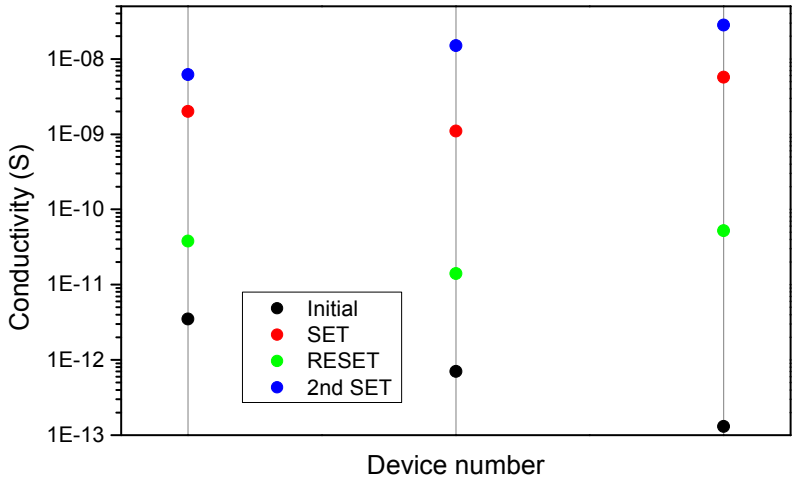

Fig. S10 Conductance of three different devices in the initial state (black), after SET (red), RESET (green) and second SET (blue), measured at 1 V.

References

1 M. A. Bryant and J. E. Pemberton, *J. Am. Chem. Soc.*, 1991, **113**, 8248–8293.

2 D. Lin-Vien, N. B. Colthup, W. G. Fateley and J. G. Grasselli, *The Handbook of Infrared and Raman Characteristic Frequencies of Organic Molecules*, Academic Press, 1991.

3 A. Zabet-Khosousi and A.-A. Dhirani, *Chem. Rev.*, 2008, **108**, 4072–4124.

4 A. Peschot, N. Bonifaci, O. Lesaint, C. Valadares and C. Poulain, *Appl. Phys. Lett.*, 2014, **105**, 123109.

5 G. Meng, Y. Cheng, K. Wu and L. Chen, *IEEE TDEI*, 2014, **21**, 1950–1956.

6 D. R. Wolters and J. J. Vanderschoot, *Philips J. Res.*, 1985, **40**, 115- 136.